Crack patterns of concrete with a single rebar subjected to non-uniform and localized corrosion

Di Qiao*, Hikaru Nakamura, Yoshihito Yamamoto, Taito Miura

Department of Civil Engineering, Nagoya University, Furo-cho, Chikusa-ku, Nagoya 464-8603, Japan

* Corresponding author

E-mail addresses: rudyqiao@gmail.com (D. Qiao), hikaru@cc.nagoya-u.ac.jp (H. Nakamura), y.yamamoto@civil.nagoya-u.ac.jp (Y. Yamamoto), t.miura@civil.nagoya-u.ac.jp (T. Miura)

Abstract: This study aims to investigate the effects of corrosion distribution, specifically non-uniform and localized corrosion, on cracks propagation in concrete. Different corrosion distributions along rebar length were simulated using a sodium chloride pond with various sizes set on the concrete cover, and a direct current was applied to accelerate the corrosion process. The test results showed that the crack pattern is more influenced by corrosion distribution than by concrete cover thickness. The cracking mechanism was analyzed using the Rigid Body Spring Method with a corrosion-expansion model, which utilized a set of experimental data relating to corrosion distribution. The crack patterns are simulated reasonably well. The analysis also indicated that the internal crack pattern is closely related to concrete surface deformation.

Keywords: crack pattern, corrosion distribution, electric corrosion test, Rigid Body Spring Method

1. Introduction

Corrosion of reinforcing steel bars (rebars) in concrete is a principal cause of deterioration of reinforced concrete (RC) structures. As forming corrosion products occupy a greater volume than that of pure steel, the resulting internal pressure can cause cracking of concrete cover. Corrosion may also lead to a loss of rebar tensile performance as a result of loss of cross section area [1], and decreased bond strength between corroded rebars and the concrete [2],

which affect the structural safety of an RC structure. Field and laboratory findings [3][4][5] suggest that the influence of rebar corrosion is more manifested by concrete cracking than the loss of structural strength. When internal cracks join together forming a spalling of concrete cover, falling concrete could be a risk to human safety. Several relevant incidents have been reported (e.g. [6]), and in some cases the cracking situation of concrete surface observed during the inspection was insignificant, which makes the prediction of internal crack propagation and potential cover spalling difficult. Therefore it is of great importance to understand how internal cracks develop due to rebar corrosion.

A number of studies have shown that corrosion-induced cracking behavior is dependent on the geometric conditions and configurations of concrete sections. Based on the bridge deck survey findings and laboratory research data, Callahan et al. [7] indicated that corrosion-caused cracks could be either inclined or horizontal in the plane of rebar, depending on cover thickness. The inclined crack may appear when concrete cover is smaller than 25.4mm, while the horizontal crack can occur when the cover thickness is greater than 31.8mm. In further analytical work, Bažant [8] suggested that the cracking resulting from rebar corrosion occurs basically in two different modes, provided that concrete with embedded rebars is a thick-walled cylinder and corrosion products distribute uniformly around the rebars. The cracking modes are related to cover thickness (C) and rebar spacing (S), as shown in **Fig. 1**. If the spacing S is greater than six times the rebar diameter (D) or the cover thickness (C) is relatively small, two cracks propagate diagonally from the rebar to the concrete surface at an angle of 45°, leading to cover spalling. If the cover thickness (C) is larger than (S-D)/2, the two cracks propagate to adjacent rebars separately, forming parallel cracks to the concrete surface resulting in delamination. In a similar way, Tsutsumi et al. [9] proposed a criterion for the internal crack patterns of single-rebar specimens based on the elastic theory that takes into consideration stress concentration, as shown in **Fig. 2**. If the value of k, which is determined by the ratio of cover-to-bar diameter (C/D), is less than three, cracks propagate diagonally to the concrete surface. If the value of k is greater than three, a vertical crack occurs in the

concrete cover along with two horizontal cracks. In addition, Caré et al. [10] studied the cracking behavior of mortar beams using an electric corrosion method, and found that the crack pattern depends upon the thickness of concrete side cover.

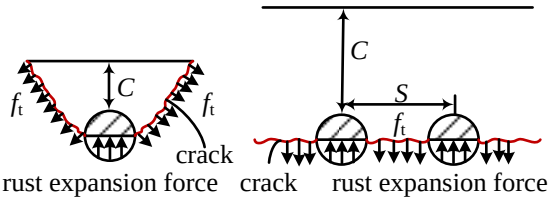

Fig. 1. Bažant's cracking mode. Adapted from [8]

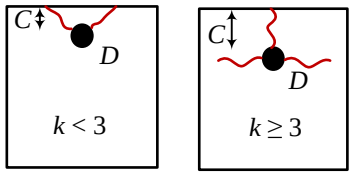

$$k = \frac{2C + D}{D}$$

Fig. 2. Tsutsumi's criterion for crack pattern. Adapted from [9]

Although the aforementioned studies provide a good understanding of corrosion-induced cracking behavior, their assumption is based on uniform corrosion around a rebar, which is different from the corrosion pattern caused by chloride attack. Yuan et al. [11][12] observed the distribution of corrosion products around the corroded rebars that were obtained by exposing the RC specimens to an artificial climate environment. Their results showed that the corrosion products only distributed on the half rebar circumference facing the concrete cover. Such corrosion generates non-uniform expansion pressure, which may cause faster development of concrete cracks than uniform corrosion [11][13][14]. The knowledge concerning the crack patterns resulting from non-uniform corrosion, however, is still limited. On the other hand, chloride penetration usually leads to localized breakdown of the passive film of a rebar, especially in the presence of initial cracks due to creep and shrinkage [15]. As a consequence, corrosion may concentrate within a small region along the length of the rebar. Previous investigations into corrosion-induced cracking behavior as referenced earlier are mostly two-dimensional studies without consideration of the localized corrosion along rebar length. Torres-Acosta and Sagüés [16] studied this problem using a dual-material rebar that was made with a carbon steel segment connected with stainless steel at both ends. The crack

patterns they observed, however, were irregular, which is possibly due to a relatively thin concrete side cover.

The present work aims to investigate the crack patterns influenced by various corrosion distributions, which can contribute to efficient maintenance work on corroded RC structures. Both experimental and numerical studies were conducted for investigation into the effects of non-uniform and localized corrosion. In the test, different corrosion distributions were obtained using an improved electric corrosion method, and the crack patterns generated were examined in detail. On the other hand, the Rigid Body Spring Method (RBSM) with the corrosion-expansion model [17] was employed to evaluate the cracking behavior, in which the corrosion distributions were assumed with test data.

2. Experimental program

The electric corrosion method with a sodium chloride (NaCl) pond built on the concrete cover was used to accelerate the corrosion process. The applicability of this method to simulate non-uniform corrosion around a rebar was firstly checked. Then different corrosion distributions along rebar length were simulated using NaCl ponds of various sizes.

2.1 Electric corrosion test

The natural corrosion process of a rebar embedded in concrete is very slow, since it may take several years for chloride ions to penetrate through concrete cover. For evaluation of structural behavior of corroded RC members, researchers thus employ several accelerating corrosion techniques to obtain the desired corrosion damage within a reasonable time frame. The techniques used include adding chlorides into the concrete mix [18][19], the electric corrosion method that is immersing the specimen in a NaCl solution and applying a direct current to the rebar [20][21], and a combination of the two methods [3][10]. The typical corrosion pattern implemented by the above techniques, however, is uniform corrosion [22]. Hence a method that can simulate non-uniform corrosion is required.

For accelerating techniques, Poursaee and Hansson [22] and Malumbel et al. [23] recommended that only selected faces of the concrete specimens should be contaminated with chlorides following the practical conditions. In this study, a 100mm wide pond filled with 3% NaCl solution was built on the concrete cover of each specimen. A copper plate was placed in the NaCl pond as the cathode. **Fig. 3** shows a diagram of the electric corrosion method. It was assumed that the corrosion current for the rebar upper part facing concrete cover would be greater than that for the lower part. This is attributable to a smaller distance from the upper part to the cathode. On the other hand, the cracks generated in concrete can cause faster chloride ingress [24], increasing the corrosion rate of the rebar upper part. Therefore, the upper part should be more corroded, showing a non-uniform corrosion pattern. A preliminary experiment was carried out to prove this point.

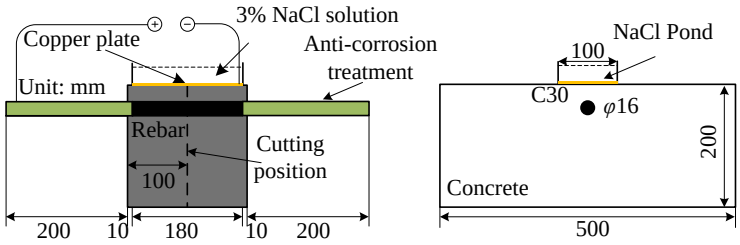

Fig. 3. Diagram of electric corrosion test

2.1.1 Test specimens of the preliminary experiment

The test included 12 prismatic concrete specimens with dimensions of 200×500×200mm^3 as shown in **Fig. 3**. In each specimen, a 600mm long round rebar with a diameter of 16mm was embedded at a depth of 30mm oriented along the 200mm length of the specimen, with exposed parts of the rebar extending 200mm beyond each end. The round rebars were used for an easy measurement of radius losses with a laser meter. Since the laser meter used has a limited scanning length of 200mm, the length of the rebar part exposed to corrosion was confined to 180mm by coating the other parts with anti-corrosion paint, waterproof tape and insulating tape in sequence to prevent from corroding. Before casting the concrete, the rebars with anti-corrosion covers were weighted for initial weights.

The concrete was made with High Early Strength Portland Cement. **Table 1** presents the mixture proportion of concrete, which was used in the entire study. The maximum diameter of the coarse aggregates used was 20mm. The volume fraction of coarse aggregates to total aggregates was 0.6. After casting, the specimens were cured in a room at 20℃ for 14 days, and then the electric corrosion test was conducted. Prior to the test, the Young's modulus, compressive strength and splitting tensile strength of the concrete were determined as 30.75GPa, 38.45MPa and 2.94MPa, respectively.

Table 1 Mixture proportion of concrete

W/C (%)	S/a (%)	Unit (kg/m^3)				
		Water	Cement	Sand	Aggregate	AE (liter/m^3)
56.5	44.0	166	294	779	990	1.18

2.1.2 Test procedures of the preliminary experiment

The corrosion time was varied as shown in **Table 2** to obtain different concrete cracking situations. The specimens were named in the form T86, meaning a period of approximately 86hours applied with a direct current. Four specimens were used for each test series, which were connected in series to a DC power and supplied with a constant current of 0.08A, as shown in **Fig. 4**. The nominal current density applied was about 900μA/cm^2, which is greater than the maximum corrosion rate recorded in real corrosion cases (100μA/cm^2 as indicated by Andrade et al. [3]). Although the current density may affect the evolution rate of surface crack width [25][26], there are no conclusive findings regarding its effect on the crack pattern. Therefore, the larger current density was used to allow quick crack generation, as referred to in other reported electric corrosion tests [11][27].

Table 2 Test variables for the preliminary experiment

Series	Testing time (hours)	Current flow (A*hr)
T86, T341, T625	86.2, 340.9, 625.0	6.9, 27.3, 50.0

Fig. 4. Electric corrosion test using NaCl ponds

After the corrosion test, one of the four specimens for each test series was cut along the center cross section for observing internal crack pattern, while the rebars embedded in the other three specimens were extracted for investigating corrosion distribution. These rebars were cleaned using a steel wire brush, and the corrosion products were removed by immersing the rebars in a 10% ammonium citrate solution for 24 hours. The mass loss Δm (g) of each rebar measured as the difference between initial weight and remaining weight was used to determine the corrosion degree η over the whole corroded area with a length of l_c:

$$\eta = \frac{\Delta m}{l_c m_u} \tag{1}$$

Where m_u is the unit mass (1.58g/mm) and l_c is the corroded length (180mm).

The radius losses of the corroded rebars were measured using the laser meter, which has a precision of 0.1μm. Various measurement lines were tested, which are located at different circumferential positions around a rebar with an interval of 30°, as shown in **Fig. 5**. The top line is the nearest side to the NaCl pond. Non-corroded parts at the sides of the corroded area were used as reference levels, with which the measured values were transformed into relative heights. The height level for each rebar was measured before the corrosion test to obtain an initial level. The difference between the initial level and the measured level after the corrosion test was treated as radius loss. Meanwhile, a Fast Fourier Transform was performed to remove the influences of imperceptible vibrations during the measurements, and then an

Inverse Fourier Transform was conducted to obtain the radius loss. Microwaves with frequencies of more than five wave periods in each 10mm of length were eliminated [28].

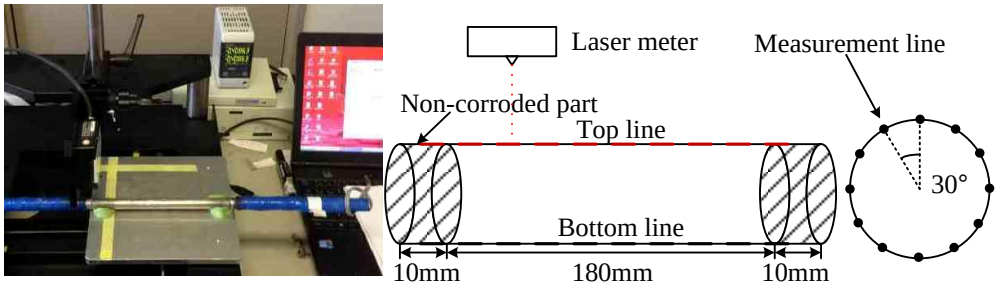

Fig. 5. Measuring radius losses by laser meter

2.1.3 Test results of the preliminary experiment

In order to clarify the corrosion pattern, the radius losses measured along the top and bottom lines are compared in **Fig. 6** (three cases for each test series), where the corrosion degrees η are also indicated. It appears that the radius losses at different positions along a measurement line are similar, demonstrating general corrosion along rebar length. With an increase of corrosion degree, the radius losses along the top line become large, while those along the bottom line barely increase. The average value for each measurement line was also calculated as shown in **Fig. 7**. Comparing the radius losses of upper circumference with those on the lower part, the difference clearly increases as corrosion develops. To some extent, this corrosion pattern is similar to that observed from the RC specimens corroded in the artificial climate environment [12]. Hence this method is capable of reproducing the non-uniform corrosion due to chloride attack. On the other hand, Malumbela et al. [29] conducted their corrosion test using a similar technique, and found that corrosion can concentrate at the rebar part under the NaCl pond when the length of the pond is comparatively smaller than that of the rebar. Therefore, the electric corrosion method with a NaCl pond set on the concrete cover was used to investigate the internal crack propagation caused by non-uniform and localized corrosion, which will be presented in the following section.

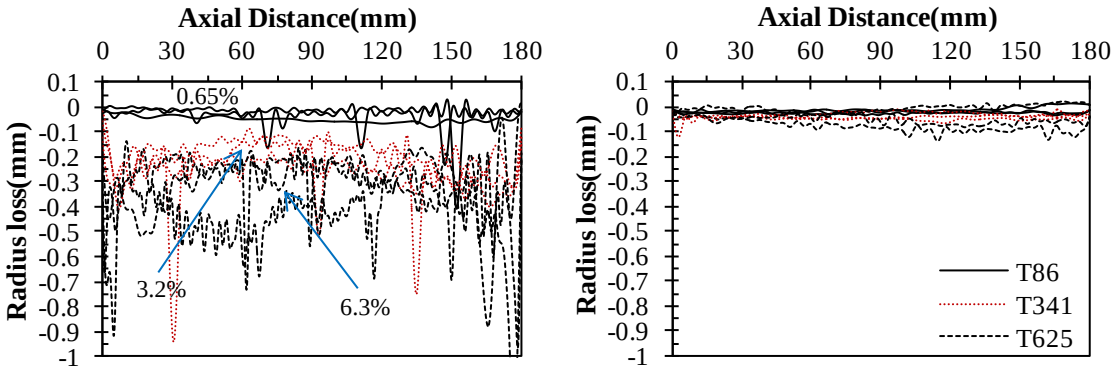

(a) Top line (b) Bottom line

Fig. 6. Radius losses along rebar length

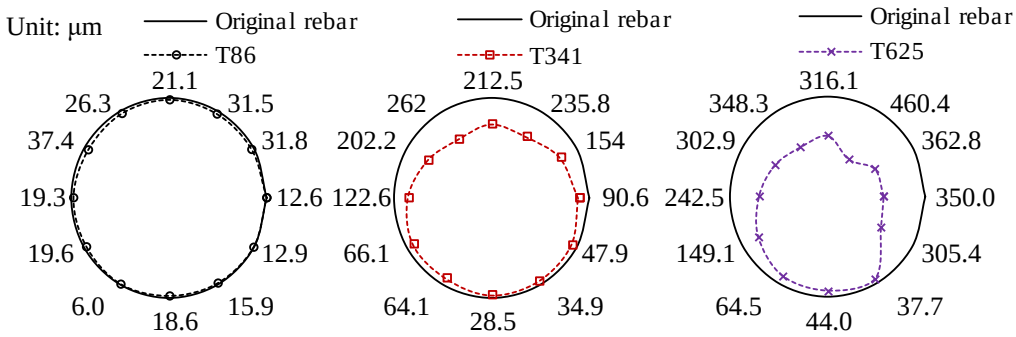

Fig. 7. Rebar cross sections after corrosion test

Fig. 8 shows the internal crack patterns observed on the center sections of the test specimens. The area of 200mm wide and 60mm in depth surrounding the rebar is magnified to clearly demonstrate the crack pattern. When the corrosion degree is comparatively small (0.65% in T86), no visible cracks can be found, and the rebar was corroded nearly uniformly (**Fig. 7**). As corrosion time increases, a vertical crack propagating from the concrete surface to the rebar and two lateral cracks were observed. The generated vertical crack provided a flow channel for chloride ions, increasing the corrosion rate of the rebar upper part (**Fig. 7)**. This suggests that the corrosion rates of various parts around a rebar could be affected by forming cracks.

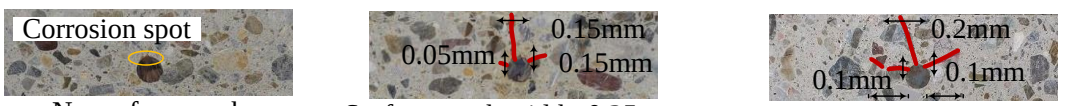

No surface crack Surface crack width: 0.25mm Surface crack width: 0.40mm

(a) T86 (b) T341 (c) T625

Fig. 8. Internal crack patterns observed in the preliminary test

2.2 Specimens for the study of crack pattern

The crack pattern is closely related to the thickness of concrete side cover [10] and the arrangement of rebars [30]. In order to remove these effects, a type of single-rebar slab specimens with dimensions of 600×500×200mm^3 was used, as shown in **Fig. 9**. A 550mm long deformed rebar with a diameter of 19mm was completely embedded in each specimen. For new RC structures, a concrete cover with minimum thickness (e.g. 50mm) is commonly required for protection of rebars from chemical attacks. This measure, however, is absent for a large number of existing structures. Since the structures with thin concrete cover were targeted in this study, two types of specimens with different cover thicknesses as 10 and 30mm were considered. The varying crack patterns as shown in **Fig. 2** were expected for these two kinds of specimens based on the crack criterion proposed by Tsutsumi et al. [9], since the *k* values are 2.05 and 4.16, respectively.

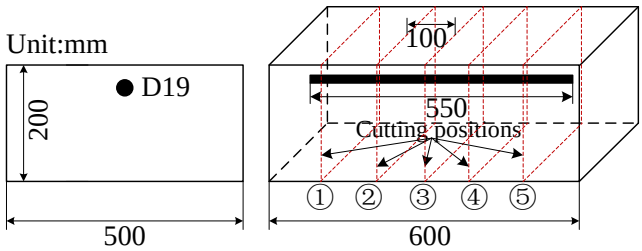

Fig. 9. Test specimens with cutting sections

A total of six specimens were cast using High Early Strength Portland Cement and coarse aggregates with a maximum diameter of 20mm. The composition of the concrete was the same as that used in the preliminary experiment, as shown in **Table 1**. Before casting, the initial mass m_0 (g) and the length l_0 (mm) of each rebar were measured to obtain the unit mass. Although the specimens were cast at different dates, they possessed similar compressive strength of about 39MPa after 14days curing as verified by tests.

2.3 Test setup for the study of crack pattern

The electric corrosion method with a NaCl pond on the concrete cover was used in this test. The nominal current density applied was 900μA/cm^2. In order to obtain various corrosion

distributions along rebar length, different ponds with length *L* varied from 500 to 100mm were used, as shown in **Fig. 10**. The cases with a 500mm long NaCl pond were designed for the study of crack pattern only affected by non-uniform corrosion. The other cases with shorter ponds were used for localized corrosion.

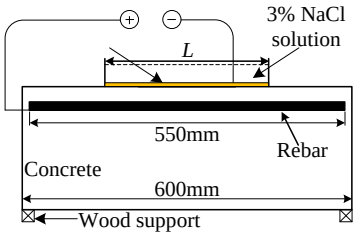

Fig. 10. Electric corrosion test for crack pattern

Table 3 shows a list of test variables. The specimen names were assigned in the form L300C30, which means a 300mm long NaCl pond set on the specimen with a 30mm thick concrete cover. In the preliminary experiment, the current efficiency determined by dividing the measured mass loss into the theoretical value given by Faraday's law was about 35%, which is smaller than that of the traditional electric corrosion method when chlorides are added into the concrete mix (nearly 100% as reported by EI Maaddawy and Soudki [26]). This is likely caused by a low concentration of chloride in the concrete. Nossoni and Harichandran [31] have reported that when the chloride content in concrete is lower than 0.5%, the current efficiency is 30-50%. Based on this knowledge, the current flow applied to the specimens with 30mm cover was 159.77A*hr, corresponding to an objective corrosion degree of 4% (an average value over the whole rebar). The current flow for the specimens with 10mm cover was a half of that for 30mm cover, considering that penetration of chloride ions through smaller concrete cover would be faster.

Table 3 Test variables for crack pattern

Specimens	Length of NaCl pond (mm)	Cover thickness (mm)	Current flow (A*hr)
L500C30, L300C30, L100C30	500, 300, 100	30	159.77
L500C10, L300C10, L100C10		10	79.89

After each corrosion test was completed, the surface crack pattern was observed. The crack widths at different positions along the rebar length direction were measured using a crack width scale, with a unit of 0.05mm. Then the specimens were cut along the sections with an interval of 100mm as show in **Fig. 9** to observe the internal crack patterns and to measure the widths and lengths of the internal cracks. The rebars were collected afterwards and cleaned using the same procedures described in the preliminary experiment. In order to obtain the corrosion distributions along rebar length, the rebar samples gathered were further cut into small segments with a length of approximately 50mm. They were weighted for the residual mass m (g) and measured for the precise length l (mm) using a vernier caliper. The corrosion degree η of each rebar segment was determined as follows:

$$\eta = \frac{m_0 l - m l_0}{m_0 l} \tag{2}$$

3. Experimental results: influence of corrosion distribution on crack pattern

3.1 Corrosion distributions

Fig. 11 shows the corrosion states of two rebar segments selected from the cases of L500C30 and L500C10 respectively. It is clear that the rebar upper part facing the concrete cover is far more corroded than the lower part.

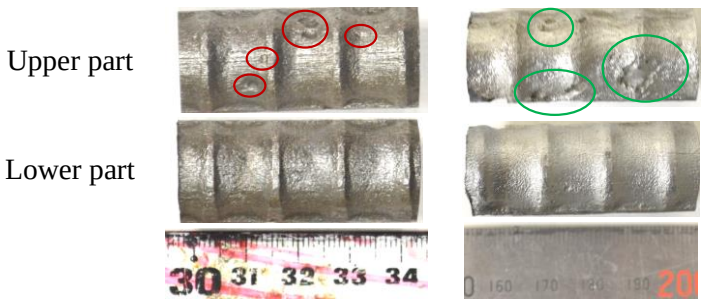

(a) L500C30 (b) L500C10

Fig. 11. Corrosion states of rebar samples

Fig. **12** shows the measured corrosion degrees against the corresponding positions along rebar length. The positions of various NaCl ponds are also indicated in the figures. The corrosion

degrees at different positions for L500C30 are all close to 3%, while in the cases of L300C30 and L100C30 the corrosion level within the area under the pond is much greater than that at the outside. For the series with 10mm cover, the corrosion distributions for L300C10 and L100C10 have similar forms to those with 30mm cover, whereas for L500C10 a relatively concentrated corrosion was observed within the 250 to 450mm part of the rebar, which is different from the even distribution obtained in L500C30. The appearance of the concentrated corrosion can be attributed to the mutual effect between cracking and corrosion, i.e. cracks enable faster transport of chlorides and water, thereby accelerating the corrosion process and causing more cracks.

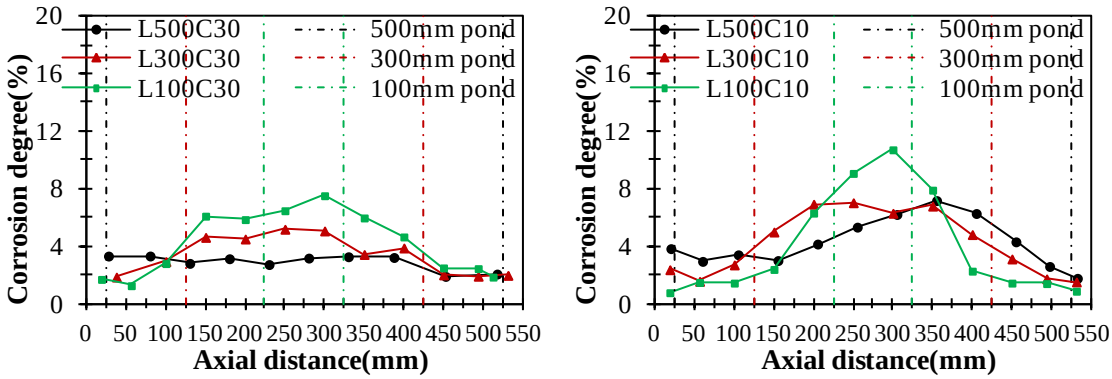

(a) C30 (159.77A*hr) (b) C10 (79.89A*hr)

Fig. 12. Measured distributions of corrosion degrees along rebar length

3.2 Crack patterns

Fig. 13 shows the surface crack patterns for L500C30 and L500C10. A single crack in the rebar length direction appeared in L500C30, which has similar crack widths (0.2-0.25mm) at different positions. For L500C10, however, multi-cracks (marked in blue) occurred in the area with concentrated corrosion as shown in **Fig. 12**. This indicates that there was an interaction between cracking and corrosion.

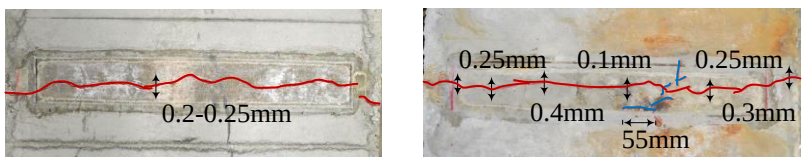

(a) L500C30 (b) L500C10

Fig. 13. Surface crack patterns for L500C30 and L500C10

The internal crack patterns observed from each cutting section (**Fig. 9**) are shown in **Fig. 14**. The figure only shows the cracked regions around the rebars, same as those in **Fig. 8**. For L500C30, the internal crack patterns on different cutting sections are nearly the same. One vertical crack connects the concrete surface to the rebar and two lateral cracks that are roughly parallel to the concrete surface propagate to the concrete sides, which form the same crack pattern as suggested by Tsutsumi et al. [9]. In the L500C10 case, the expected internal crack pattern that consists of two inclined cracks only appeared on the section ④, while the other four sections all showed a crack pattern consisting of a vertical crack, a small inclined crack and two nearly horizontal cracks. This result demonstrates that besides cover thickness, the internal crack pattern may be affected by corrosion distribution around a rebar.

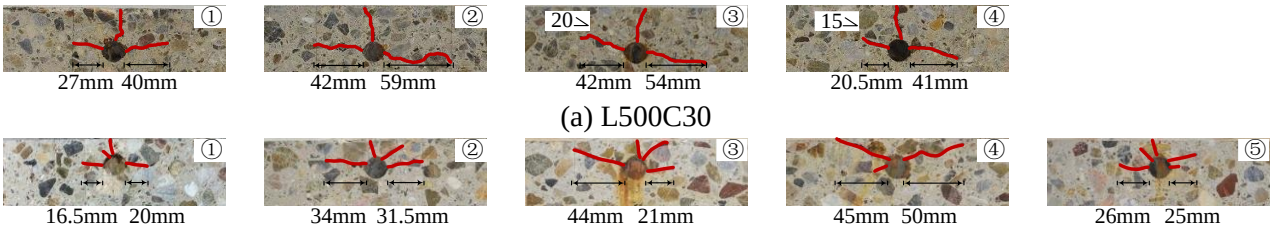

(a) L500C30

(b) L500C10

Fig. 14. Internal crack patterns for L500C30 and L500C10

Fig. 15 shows a comparison of surface crack patterns between different test cases with short NaCl ponds. For cases with 30mm cover, a longitudinal crack appeared on the concrete surface, which is similar to the crack situation of L500C30. Comparing the crack widths at different positions, however, we found that the width within the area under the pond is smaller than those at the external areas. Taking L300C30 as an example, the surface crack width is about 0.2-0.25mm on the center part, but doubles at the sides. Given that the corrosion level on the center part is much higher, it can be assumed that the internal crack propagation is dominant in the cracking process. In the cases with 10mm cover, a primary longitudinal crack was also observed, suggesting a vertical crack occurring inside concrete. The crack width at the center part is similarly smaller than those at the areas outside the pond. Moreover, a number of secondary cracks with a width of 0.05mm appeared near the pond

(marked in blue) due to the propagation of internal cracks to the concrete surface. These results suggest that localized corrosion may lead to significant development of internal cracks.

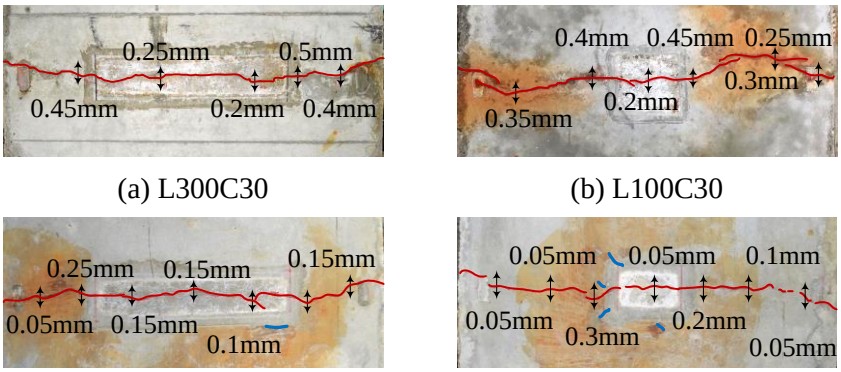

(a) L300C30 (b) L100C30

(c) L300C10 (d) L100C10

Fig. 15. Surface crack patterns under localized corrosion along rebar length

Fig. 16 shows the internal crack patterns observed on different cutting sections for cases with short NaCl ponds. A very interesting phenomenon of cracks propagation can be found by comparing the internal crack patterns with those in L500C30 and L500C10. For cases with 30mm cover, only vertical cracks occurred in the region distant from the NaCl pond, where the corrosion degree is relatively small. On the other hand, in region near the pond two lateral cracks having large crack width appeared as well. Moreover, one lateral crack inclines to the concrete surface at an angle between 30° - 45°. Provided that the corrosion amounts are sufficient, the vertical crack that penetrates through the concrete cover together with the lateral crack that propagates diagonally to the concrete surface tends to form a fracture plane, which can be considered to represent the cover spalling. The cases with 10mm cover showed a similar cracking behavior, i.e. the internal crack patterns varied with the observing sections, and the inclined lateral cracks appeared in the area near the NaCl pond, demonstrating a potential for cover spalling. From these results, it is clear that the concentrated corrosion along rebar length can cause the lateral crack to incline to the concrete surface, which also explains the occurrence of a different crack pattern on section ④ of L500C10 as shown in Fig. **14**.

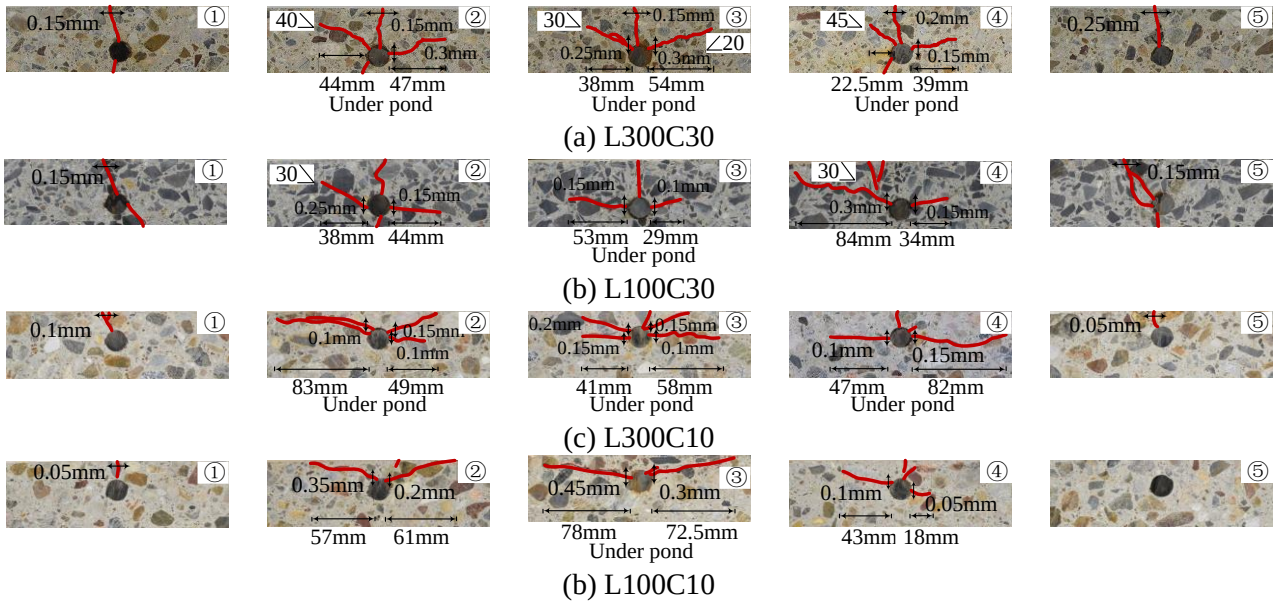

Fig. 16. Internal crack patterns under localized corrosion along rebar length

4. Numerical evaluation of corrosion induced cracking behavior

The experimental results suggest that the corrosion-induced crack pattern depends on how corrosion distributes around or along a rebar. In this section, a numerical analysis is performed to analyze the crack patterns for various corrosion distributions, and to clarify the cracking mechanism. The RBSM with the corrosion-expansion model [17] was applied in the analysis.

4.1 Numerical model

4.1.1 Three-dimensional RBSM

The RBSM as a discrete numerical approach represents a continuum material as an assemblage of rigid particle elements interconnected by zero-length springs along their boundaries, as shown in **Fig. 17**. The elements are randomly generated with Voronoi Diagram. Each of the elements has six degrees of freedom at its nucleus. At the center point of every triangle formed by the center of gravity and the vertices of the boundary between two elements, three springs, one normal and two shear springs are defined. Nonlinear material models of concrete [6] were introduced into the springs. The response of the spring model provides an understanding of the interaction between particle elements instead of the internal behavior of each element based on continuum mechanics. In a RBSM model, cracks appear at

the boundaries between adjacent rigid particles, and the crack width can be automatically calculated as a relative displacement between the centers of the particles, which facilitate the simulation of crack pattern. The three-dimensional RBSM developed by Yamamoto et al. [32] was used in this study. The material parameters of concrete were determined by tension and compression simulations of a standard cylinder, which were compared with test data.

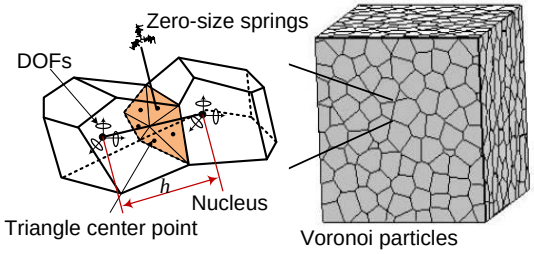

Fig. 17. Voronoi particle definition of RBSM element

4.1.2 Corrosion-expansion model

The volume expansion of corrosion products was modeled by internal expansion pressure, as shown in **Fig. 18**. A three-phase material model consisting of rebar, concrete, and corrosion products was established. The rebar was modeled as linear elastic with an elastic modulus of 200GPa. The concrete was treated as a homogeneous material without inclusions of individual coarse aggregates. Although Pan and Lu [33] and Šavija et al. [14] suggested that the distribution of aggregates may affect the penetration route of a crack, e.g., if a coarse aggregate happened to locate in front of the crack tip, the crack propagation would not be straight forward, the experimental results presented above show no appreciate effect on the macroscopic crack pattern. This is likely due to the controlled maximum aggregate size compared with the concrete cover thickness. We consider that the crack patterns predicted by the corrosion-expansion model are reliable owing to the random geometry of the RBSM model. The corrosion products layer was modeled with an elastic material model, which has a constant thickness (H). The former work by Tran et al. [17] showed that, when H is assumed as 1.0mm and the elastic modulus (E_r) of corrosion products as 500MPa, the model simulates reasonable cracking behavior in comparison with the test results. These assumptions have also been adopted herein.

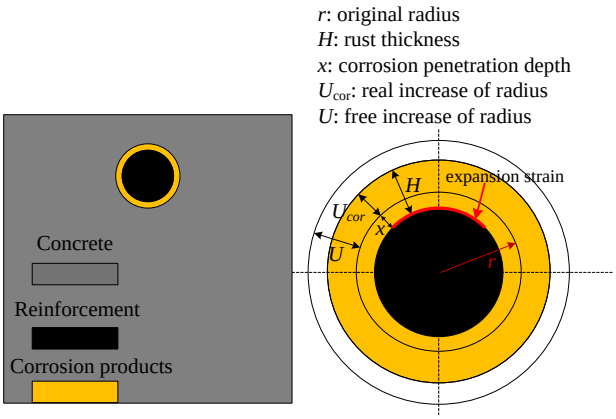

Fig. 18. Corrosion-expansion model

The increment of expansion stress for each analysis step was determined as:

$$\Delta\sigma_{cor} = E_r\left(\Delta\varepsilon - \Delta\varepsilon_0\right) = E_r\left(\frac{\Delta U_{cor}}{H} - \frac{\Delta U}{H}\right) \tag{3}$$

Where ΔU_{cor} is an increment of the real increase of rebar radius corresponding to the confinement of concrete, and ΔU is an increment of the free increase of rebar radius.

Considering the nature of corrosion expansion, we assumed the internal expansion pressure is only activated in the normal direction. The expansion stress is thus applied only to the normal springs on the boundary between the corrosion products layer and the rebar. The shear stiffness for shear springs of the corrosion products layer was set nearly zero to model free sliding of the corrosion products layer in the shear direction. In the analysis, the expansion stress was solved using the initial strain problem with an increment of initial strain ($\Delta U/H$) in each step. The accumulative U was determined by the input corrosion degree η:

$$U = \frac{\eta \cdot r \cdot \left(\alpha_{cor} - 1\right)}{2} \tag{4}$$

Where r is the original rebar radius, and α_{cor} is the volume-expansion ratio of corrosion products, which was assumed as 2.5. As concrete cracking is sensitive to the transient stress state in the analysis, the ΔU applied in each step should be kept small enough to obtain a converged solution. The increment of corrosion degree $\Delta\eta$ (%) as input data was set to 0.02 to ensure a small ΔU.

4.1.3 Modeling of non-uniform corrosion

The test results of the preliminary experiment presented in section 2.1.3 show that the rebar part near cracks is more corroded than that surrounded by uncracked concrete. Taking account of the effect of forming cracks on corrosion process, non-uniform corrosion after crack initiation was assumed as shown in **Fig. 19**. When a vertical crack with a width greater than 0.1mm appears in the concrete cover, the corrosion products are only distributed in the upper part [17]. The angle θ was used to represent the distribution of corrosion products around a rebar. Correspondingly, the increment of initial strain was only applied in that area, while the average corrosion degree was the same as that in the uniform corrosion model.

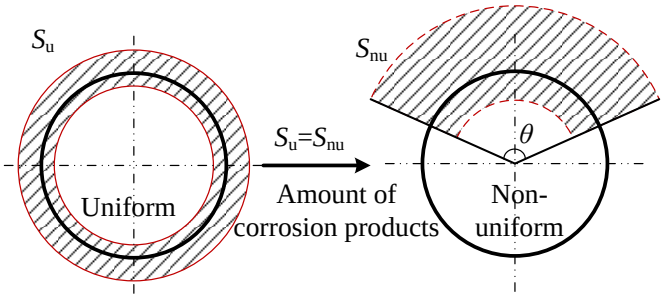

Fig. 19. Non-uniform corrosion model

4.2 Analysis of crack propagation due to non-uniform corrosion

In order to confirm the key parameter θ for the non-uniform corrosion model, the cases of L500C30 and L500C10 were analyzed and the internal crack patterns modeled were compared with the test results. The RBSM model created has the same dimension as that of the test specimens, as shown in **Fig. 20**. The mesh size of the Voronoi particles near the rebar is either 5 or 2mm for 30 and 10mm concrete cover, while the mesh size in the outer area is 30mm. In the analysis, the angle θ was ranged from 360° to 45°, in which 360° represents uniform corrosion around the rebar. The concentrated corrosion along rebar length that occurred in the L500C10 case was not considered for investigation of the effect of non-uniform corrosion. Hence the corrosion amounts were distributed evenly along rebar length.

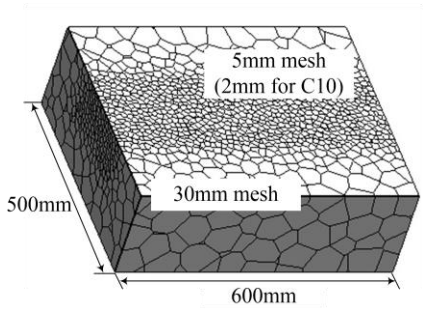

Fig. 20. 3D view of RBSM model

Fig. 21 shows the simulated crack patterns under a corrosion degree of 3%, corresponding to the value measured in the test (**Fig. 12**). The region surrounding the rebar with dimensions of 200×60mm^2 is focused. The cracks are plotted in different colors, i.e., the yellow and red ones denote the cracks with widths greater than 0.1 and 0.3mm, respectively. The lateral crack length is the horizontal distance calculated from the side of the rebar to the tip of the crack. It appears that the non-uniform corrosion (θ<360°) results in more cracks than the uniform corrosion (θ=360°), which are more close to the cracking situations observed in the tests (**Fig. 14**). Therefore, non-uniform corrosion should be considered for evaluation of the cracking behavior due to chloride-induced corrosion. For L500C30, when θ equals 90°, the crack pattern modeled agrees with the test result and the calculated lateral crack length is also similar. For L500C10, it seems that the internal crack pattern is sensitive to the corrosion distribution. When θ is greater than 120°, two parallel cracks to the concrete surface were observed, which is in agreement with the test result. On the other hand, when θ is smaller than 120°, the lateral cracks were observed to incline to the concrete surface. This shows that the corrosion-expansion model can accurately simulate internal crack pattern, if the corrosion distribution is properly assumed.

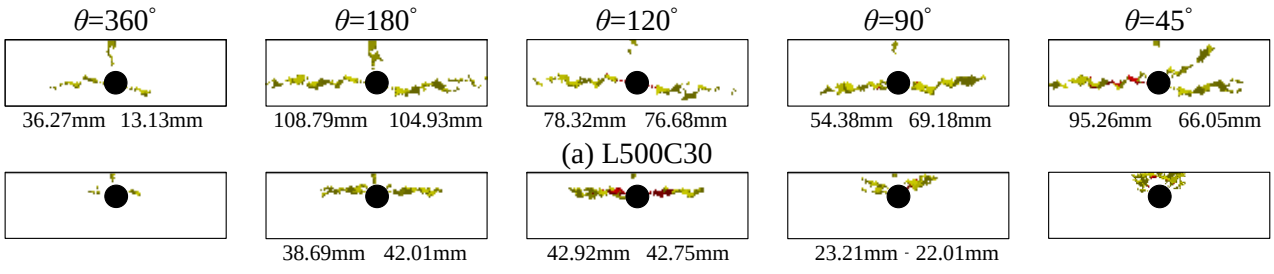

Fig. 21. Simulated internal crack patterns for L500C30 and L500C10

Fig. 22 presents the development of surface crack width against corrosion degree for the series with 30mm cover. It was found that when θ equals 180°, surface crack develops more rapidly than that for uniform corrosion (θ=360°). It is because that the corrosion products were only distributed in the half circumference facing the concrete cover, causing greater expansion pressure. When the corrosion area further concentrates (θ<120°), the evolution rate, however, becomes lower due to the change of the internal crack pattern, i.e. the occurrence of the inclined lateral cracks (θ=45°).

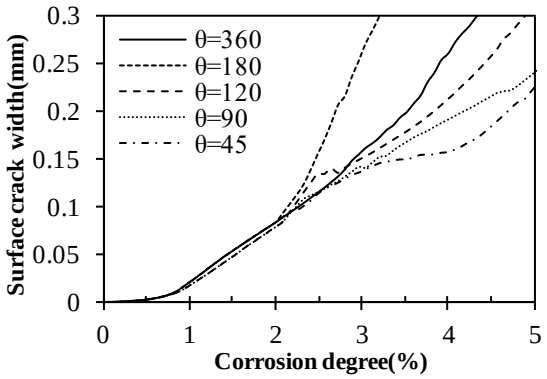

Fig. 22. Surface crack evolution for various corrosion distributions (C30)

4.3 Analysis of crack propagation due to localized corrosion

In the analysis of localized corrosion, the corrosion amounts along the rebar were predefined based on the values measured in the tests (**Fig. 12**). A simple trapezium of corrosion distribution along rebar length was assumed as shown in **Fig. 23**, where the flat part with a high corrosion level represents the area under the NaCl pond. These predefined local corrosion degrees were used to determine the initial strains for cracking analysis based on Eq. (3) and Eq. (4). In the circumferential direction of the rebar, the non-uniform corrosion process was assumed (**Fig. 19**). The parameter θ was set to 90° and 180° for cases with 30 and 10mm cover respectively, which was based on the corrosion states in **Fig. 11** and the model verification in **Fig. 21**.

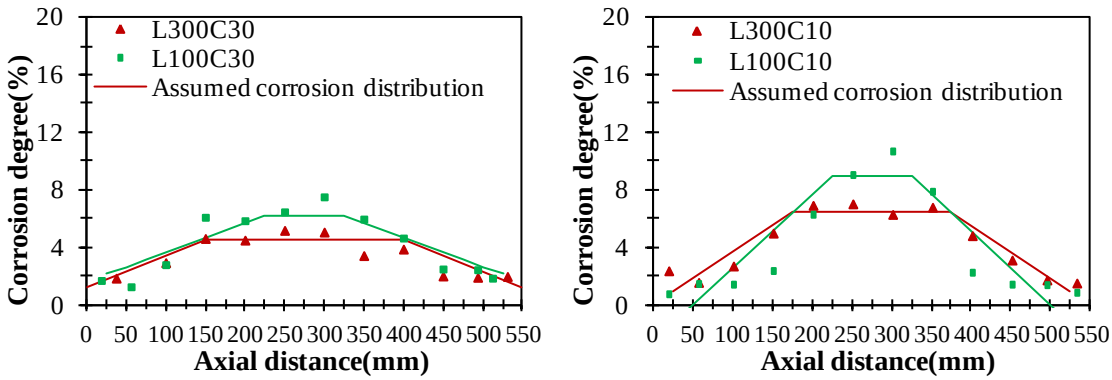

(a) C30 (b) C10

Fig. 23. Assumed corrosion distributions for analysis

The surface crack patterns modeled for cases with shorter ponds are shown in **Fig. 24**. A longitudinal crack with varied crack widths at different positions can be confirmed in the analysis. In the cases with 10mm cover, a number of small cracks near the NaCl pond were also observed. When compared with the test results (**Fig. 15**), it seems that the crack widths on the area outside the pond are rather smaller than those on the center part under the pond. The reason for this difference between the simulations and the experimental results is not clear, which requires more future work.

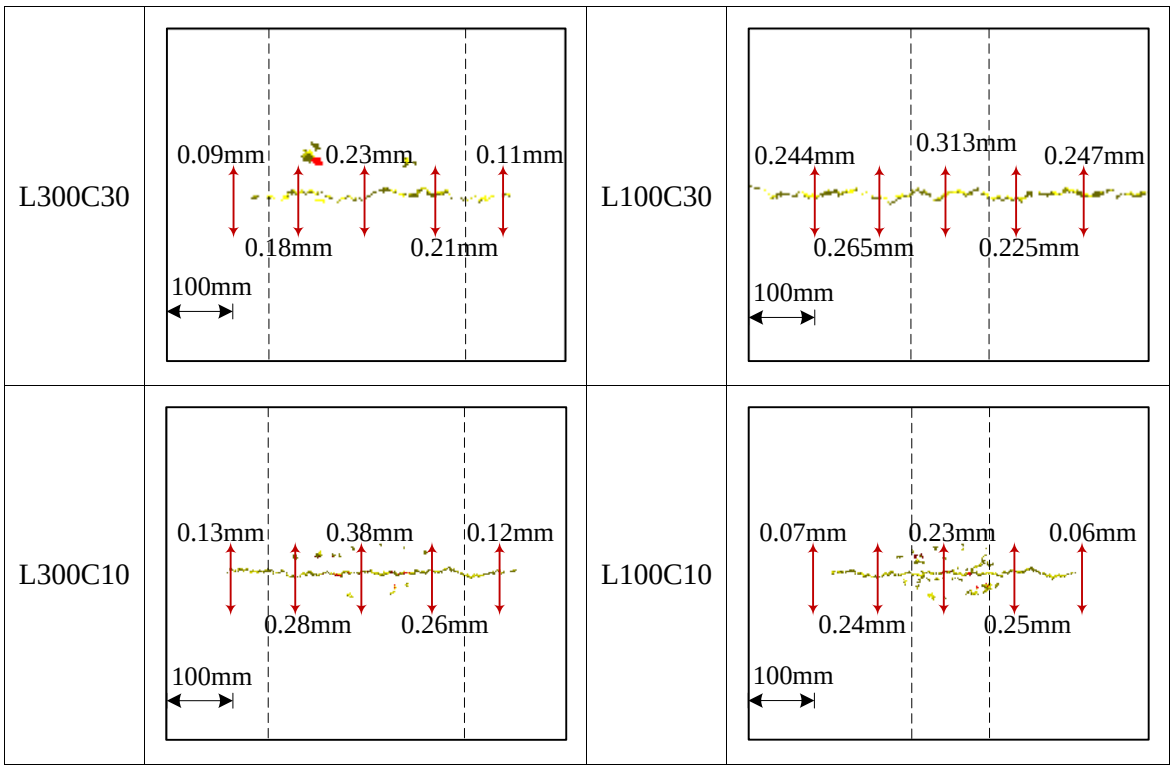

Noted: ------- Position of NaCl pond

Fig. 24. Simulated surface crack patterns under localized corrosion along rebar length

Fig. 25 shows the simulated internal crack patterns, in which the cracks plotted in green have a width of 0.05-0.1mm. Five cross sections with a distance of 100mm were examined, corresponding to the cutting sections described in **Fig. 9**. It was observed that modeled internal crack patterns changed in each cutting section. The observed development of lateral cracks was more profound near the NaCl pond. Furthermore, in the cases with 30mm cover a lateral crack propagates in a diagonal way and almost reaches the concrete surface. In the cases with 10mm cover, two wide inclined cracks were also observed. The inclined cracks together with the vertical crack can form a fracture plane causing cover spalling. These results agree well with the observations in the test, proving that concentrated corrosion along rebar length may lead to cover spalling.

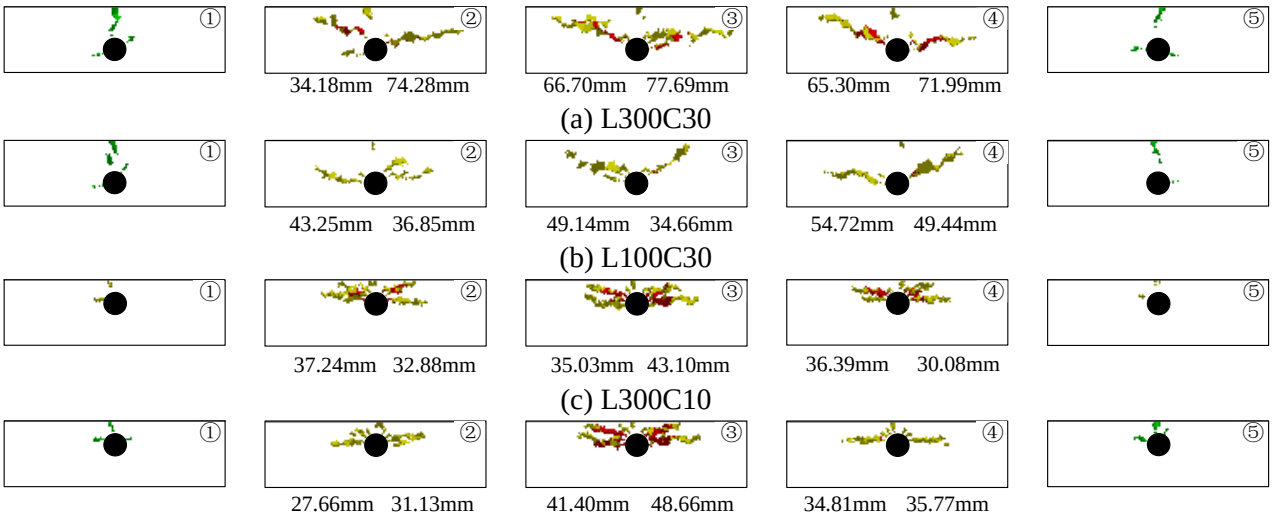

Fig. 25. Simulated internal crack patterns under localized corrosion along rebar length

Fig. 26 shows a comparison of surface deformation between different cases with 30mm cover on the basis of corrosion level of 3%. It is clear that the surface deformation areas for localized corrosion (L300C30 and L100C30) are smaller than that for general corrosion (L500C30). The deformation values at three different places, corresponding to the cutting sections of ①, ② and ③ (**Fig. 9**), are compared in **Fig. 27**. For general corrosion (L500C30) the surface deformation is consistent at different places, whereas for localized corrosion the deformation at the area with a lower corrosion degree (section ①) is significantly smaller

than that with a higher corrosion degree (section ③). This inconsistency of deformation rate causes a limited deformation for the center part of concrete cover, which is manifested by a decrease of the deformation area along the transverse direction as well as a reduction of the maximum deformation value compared with that for general corrosion. As a result, the lateral cracks incline to the concrete surface.

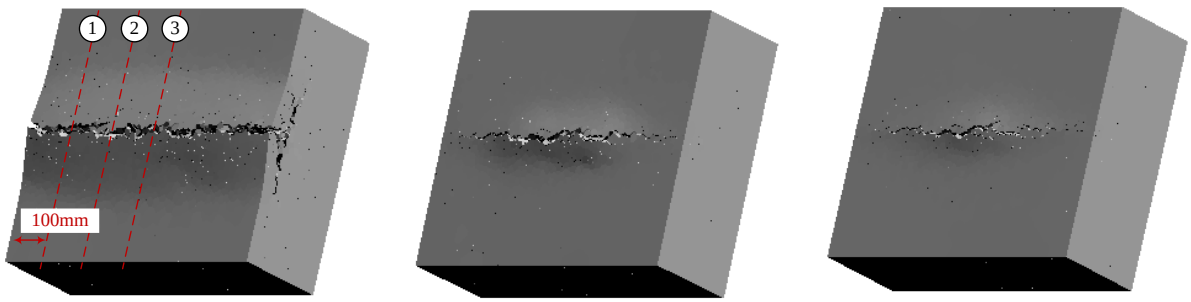

(a) L500C30 (b) L300C30 (c) L100C30

Fig. 26. Deformation under various corrosion distributions (magnification × 50)

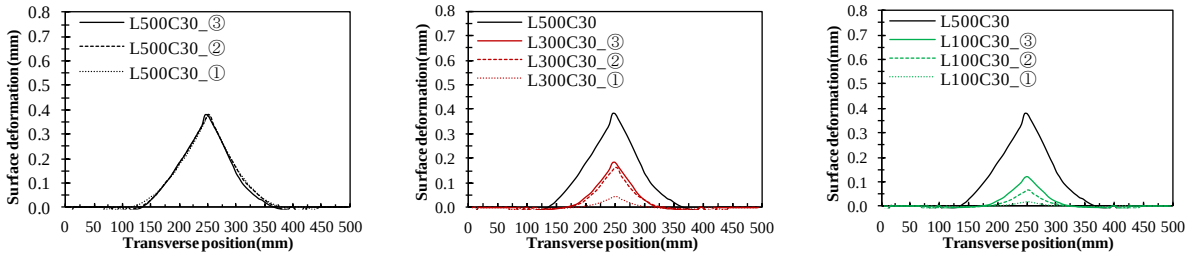

(a) L500C30 (b) L300C30 (c) L100C30

Fig. 27. Comparison of surface deformation between various corrosion distributions

4.4 Discussion

The simulation results demonstrate that the corrosion-caused crack pattern is highly dependent on corrosion distribution. In case of non-uniform corrosion, if a rebar is broadly corroded in the circumferential direction, the resulting internal crack pattern for 10mm cover is similar to that for 30mm cover, which consists of parallel cracks to the concrete surface; if the corrosion concentrates significantly in the area facing concrete cover, the internal cracks for 30mm cover may also incline to the concrete surface. These findings contradict the concept of the cracking modes developed using the thick-walled cylinder theory (Bažant [8]; Tsutsumi et al. [9]), i.e. the internal crack pattern for a given rebar diameter is determined by

concrete cover thickness. On the other hand, the crack pattern due to localized corrosion varies along rebar length. In the area with concentrated corrosion, the lateral cracks incline to the concrete surface rather than propagate horizontally to the concrete sides, triggering cover spalling. Outside this area only vertical cracks appear. Therefore, the corrosion distribution should be taken into consideration for evaluation of internal cracking situations.

The numerical analysis also offers an implication for the assessment of corrosion-caused damage using surface crack width. Non-uniform and localized corrosion may lead to great development of internal cracks without a discernible sign in the surface crack width. Therefore, it is inappropriate to assess corrosion extent and internal cracking situation based on surface crack width alone. Additionally, non-uniform and localized corrosion may cause the lateral cracks inside concrete to incline to the concrete surface. These inclined cracks are often more dangerous because they can help to accelerate the corrosion process and also induce cover spalling [8]. This phenomenon may occur in a concrete cover as thick as 30mm, which is normally considered to be safe.

5. Conclusions

The purpose of this study is to investigate the crack patterns resulting from non-uniform and localized corrosion, which was studied both experimentally and numerically. The following conclusions can be derived from this study:

(1) The electric corrosion method with a NaCl pond on the concrete cover is capable of simulating the corrosion pattern due to chloride attack that is corrosion concentrates at the half circumference facing concrete cover. The measured radius losses around the rebars showed that the cracks generated in concrete may lead to an increase of corrosion rate for the rebar part nearby. The use of a short pond can result in a relatively high corrosion level under the pond.

(2) The test results showed that in case of non-uniform corrosion the internal crack patterns for 10 and 30mm covers may both consist of parallel cracks to the concrete surface. In case of localized corrosion along rebar length, the resulting internal crack pattern varies

with the observing sections along rebar length: in section with concentrated corrosion, the inclined lateral cracks appear instead of the parallel cracks, causing cover spalling; in the other sections with less rebar corrosion, only vertical cracks occur. The applicability of the crack modes based on the thick-walled cylinder theory is limited since they do not consider the influence of corrosion distribution.

(3) The RBSM with the corrosion-expansion model can simulate reasonable crack patterns in comparison with the test results, if the corrosion distribution is properly assumed.

(4) The analysis of the effect of non-uniform corrosion indicates that internal crack propagation is dependent on corrosion distribution rather than cover thickness. If corrosion distributes broadly around a rebar, the parallel cracks also occur for 10mm cover.

(5) The analysis of the effect of localized corrosion clarifies that the occurrence of inclined lateral crack can be attributed to confined concrete surface deformation.

(6) Non-uniform and localized corrosion can create severe internal damage without a noticeable surface cracking. Such phenomenon must be considered in the condition assessment of RC structures exposed to chloride-laden environment.

References

[1] Cairns J, Plizzari GA, Du YG, Law DW, Franzoni C. Mechanical properties of corrosion-damaged reinforcement. ACI Mater J 2005; 102(4): 256-264.

[2] Lundgren K. Modeling the effect of corrosion on bond in reinforced concrete. Mag Concr Res 2002; 54(3): 165-173.

[3] Andrade C, Alonso C, Molina FJ. Cover cracking as a function of bar corrosion: Part I – Experimental test. Mater Struct 1993; 26: 453-464.

[4] Li CQ. Life-cycle modeling of corrosion-affected concrete structures: propagation. J Struct Eng - ASCE 2003; 129(6): 753-761.

[5] Torres-Acosta AA, Martínez-Madrid M. Residual life of corroding reinforced concrete structures in marine environment. J Mater Civ Eng 2003; 15(4): 344-353.

[6] Tran KK. Study on cracking behavior of concrete due to rebar corrosion. PhD Thesis, Nagoya, Nagoya University, 2012.

[7] Callahan JP, Lott JL, Kesler CE. Bridge deck deterioration and crack control. J Struct Div - ASCE 1970; 96(10): 2021-2036.

[8] Bažant ZP. Physical model for steel corrosion in concrete sea structures – Application. J Struct Div - ASCE 1979; 105(ST6): 1155-1166.

[9] Tsutsumi T, Matsushima M, Murakami Y, Seki H. Study on crack models caused by pressure due to corrosion products. Doboku Gakkai Ronbushu 1996; 30(2): 159-166 [in Japanese].

[10] Caré S, Nguyen QT, Beddiar K, Berthaud Y. Times to cracking in reinforced mortar beams subjected to accelerated corrosion tests. Mater Struct 2010: 43: 107-124.

[11] Yuan Y, Ji Y, Shah SP. Comparison of two accelerated corrosion techniques for concrete structures. ACI Mater J 2007; 104(3): 344-347.

[12] Yuan YS, Ji YS. Modeling corroded section configuration of steel bar in concrete structure. Constr Build Mater 2009; 23: 2461-2466.

[13] Du YG, Chan AHC, Clark LA. Finite element analysis of the effects of radial expansion of corroded reinforcement. Comput Struct 2006; 84: 917-929.

[14] Šavija B, Luković M, Pacheco J, Schlangen E. Cracking of the concrete cover due to reinforcement corrosion: a two-dimensional lattice model study. Constr Build Mater 2013; 44: 626-638.

[15] Bertolini L, Elsener B, Pedeferri P, Polder RB. Corrosion of steel in concrete. Germany: Wiley-VCH, 2004.

[16] Torres-Acosta AA, Sagüés AA. Concrete cracking by localized steel corrosion – geometric effects. ACI Mater J 2004; 101(6): 501-507.

[17] Tran KK, Nakamura H, Kawamura K, Kunieda M. Analysis of crack propagation due to rebar corrosion using RBSM. Cem Concr Compos 2011; 33(9): 906-917.

[18] Treadaway KWJ, Cox RN, Brown BL. Durability of corrosion resisting steels in concrete. ICE Proc 1989; 86(2): 305-331.

[19] Liu YP, Weyers RE. Modeling the time-to-corrosion cracking in chloride contaminated reinforced concrete structures. ACI Mater J 1998; 95(6): 675-681.

[20] Grimes WD, Hartt WH, Turner DH. Cracking of concrete in sea water due to embedded metal corrosion. Corros 1979; 35(7): 309-316.

[21] Caré S, Raharinaivo A. Influence of impressed current on the initiation of damages in reinforced mortar due to corrosion of embedded steel. Cem Concr Res 2007; 37: 1598-1612.

[22] Poursaee A, Hansson CM. Potential pitfalls in assessing chloride-induced corrosion of steel in concrete. Cem Concr Res 2009; 39: 391-400.

[23] Malumbela G, Moyo P, Alexander M. A step towards standardizing accelerated corrosion tests on laboratory reinforced concrete specimen. J S Afr Inst Civ Eng 2012; 54(2): 78-85.

[24] Djerbi A, Bonnet S, Khelidj A, Baroghel-bouny V. Influence of traversing crack on chloride diffusion into concrete. Cem Concr Res 2008; 38: 877-883.

[25] Alonso C, Andrade C, Rodriguez J, Diez JM. Factors controlling cracking of concrete affected by reinforcement corrosion. Mater Struct 1998; 31: 435-441.

[26] El Maaddawy T, Soudki K. Effectiveness of impressed current technique to simulate corrosion of steel reinforcement in concrete. J Mater Civ Eng 2003; 15(1): 41-47.

[27] Mangat PS, Elgarf MS. Flexural strength of concrete beams with corroding reinforcement. ACI Struct J 1999; 96(1): 149-158.

[28] Mada T. Automatic Fourier analysis by EXCEL. Tech Rep Tech Serv Div, Res Inst Appl Mech, Kyushu University 2011; 12: 1-8 [in Japanese].

[29] Malumbela G, Moyo P, Alexander M. Influence of corrosion crack patterns on the rate of crack widening of RC beams. Constr Build Mater 2011; 25(5): 2540-2553.

[30] Kawamura K, Tran KK, Nakamura H, Kunieda M. Surface crack propagation behavior against the surface deformation and inside cracks due to rebar corrosion. Proc JCI 2010; 32: 1007-1012 [in Japanese].

[31] Nossoni G, Harichandran R. Current efficiency in accelerated corrosion testing of concrete. Corros 2012; 68(9): 801-809.

[32] Yamamoto Y, Nakamura H, Kuroda I, Furuya N. Analysis of compression failure of concrete by three-dimensional rigid body spring model. Doboku Gakkai Ronbunshu 2008; 64(4): 612-630 [in Japanese].

[33] Pan TY, Lu Y. Stochastic modeling of reinforced concrete cracking due to nonuniform corrosion: FEM-based cross-scale analysis. J Mater Civ Eng 2012; 24(6): 398-706.